Small fast inkdrop emission from a nozzle

Problem presented by

Steve Temple

Xaar plc, Cambridge

Problem statement

In the normal operation of ink jet printheads, ink drops are extruded through a nozzle, producing plugs with the same diameter as the nozzle. However, Xaar has observed that under certain circumstances a smaller, faster drop is emitted from the centre of the nozzle, having about one quarter the diameter of the nozzle and about twice the velocity of normal operation. The Study Group was asked to consider possible mechanisms that could lead to this unusual behaviour. If the production of such microdrops can be understood, a practical design might be viable, so allowing printing with much higher resolution and with reduced ink usage.

Study Group contributors

James Healy (University of Southampton)
John Hinch (University of Cambridge)
Sam Howison (University of Oxford)
Hilary Ockendon (University of Oxford)
John Ockendon (University of Oxford)
David Parker (Univerity of Edinburgh)
Colin Please (University of Southampton)
Christopher Voyce (University of Southampton)

Report prepared by

Sam Howison (University of Oxford)
John Ockendon (University of Oxford)
David Parker (University of Edinburgh)

1 Problem description

1.1 Circulated description

The following description was prepared by Steve Temple of Xaar and circulated in advance of the Study Group.

> In firing ink jet printheads, we have observed from time to time that it is possible to create a drop much smaller than the nozzle. In normal operation of Xaar Printheads, the drop ejected is first extruded through the nozzle by a positive pressure. This results in a forward moving plug having a certain momentum and of the diameter of the nozzle. At the end of a time period (typically between 2 and 10 μsec, according to the detailed design), the pressure is reversed and a neck begins to form at the nozzle. The momentum of the plug carries it forward, extending the neck to eventually become a long ligature, which finally breaks off at the nozzle. Break-off occurs between 10 and 100 μsec after the pressure reversal, and this time is easily predicted with a slight modification to the Rayleigh break off criterion.
>
> However, under certain circumstances, not really known in the sense of my being able to repeat them, we have seen a quite different behaviour in which a much smaller drop — *e.g.* $\frac{1}{4}$ the diameter of the nozzle emerges rather suddenly from the centre of the nozzle and flies off at typically 2$\times$ the normal firing velocity. We believe that this is associated with very short pressure pulses — of the order of 1 μsec — but usually it happens as a result of reflected acoustic waves and not as a result of controlling the applied pressure; hence the difficulty of reproducing the circumstances.
>
> In a paper 'Micro-machined acoustic-wave liquid ejector' [1], a focussed acoustic wave technique is described which gives rise to a droplet in a similar fashion from the centre of a free surface. I believe this may be relevant, though there is no actuator element in our system corresponding to the one described.
>
> Our actuator consists of a piezo-electric channel of a defined length which squeezes the ink and creates a nominally plane acoustic wave which impinges on the nozzle. Any focussing which takes place must be due entirely to the shape of the nozzle.
>
> I believe that radial acoustic waves are dispersive, and it might be that we accidentally create a soliton, which propagates radially within the nozzle causing the energetic ejection. Normally such waves would disperse; hence my suggestion that a soliton may be involved.
>
> Really, this exhausts my current knowledge on the subject (and I do not understand solitons!). I can describe our current actuator in more detail, but I feel that it is probably better at this stage to keep the minds open and allow an element of imagination to take charge!

1.2 Notes of presentation to the Study Group

The Xaar patented technology was described, in which the channel walls are of poled PZT (lead zirconate titanate) operated in its shear mode. To fire a channel normally, the walls are first opened to take in more ink, then squeezed to eject the droplet, then returned to the neutral state. Each wall is shared between the channels either side of it, so, to avoid unintentional firing of neighbouring channels, any channels fired simultaneously must have at least 2 inactive channels between them. Thus if the channels are labelled ABCABCABC..., the A channels are fired, then the B, then C, then A *etc.* In fact B and C are fired before the ligature to A breaks off. Xaar's current model for the action includes the propagation of acoustic waves in the channel, reflection from the nozzle and reservoir ends, and treats the droplet during ejection as having a head that carries the mass and momentum, and a ligature that provides a viscoelastic braking force until it ruptures. The droplet size can be 3–6 pl, corresponding to a droplet radius of about 10 μm. 'Greyscales' can be achieved by modulating the droplet size. A sideshooter system was also described, having the advantages that a slow circulating flow helps to clean and cool the nozzle.

Currently 'microdrop' emission can be assured only in very narrow parameter regimes. If the production of microdrops could be better understood, a practical design might be viable, so allowing printing with much higher resolution and with reduced ink usage. Xaar would like to know why and when the microdrop is emitted. The normal droplet ejection velocity is 10 m/s, but the microdrop velocity is about 20 m/s or more. In general terms, the microdrop is observed in circumstances when Xaar expect to generate a sharp acoustic pulse — a spike, lasting for 1–2 μs, of perhaps 5–6 atmospheres. The nozzle diameter is about 20 μm, the normal droplet diameter comparable to this, and the microdroplet diameter about $\frac{1}{4}$ of this. The behaviour of the ink meniscus was described: after ligature break-off it normally has an appearance roughly as the first diagram below, and then oscillates (in the channel direction) as it returns to its equilibrium state. However, the action occasionally departs from symmetry, roughly as the second diagram, in which case there are also transverse oscillations of the meniscus.

Figure 1: Schematic diagram of asymmetric break-off.

2 Paradigm problem

The basic problem is to adapt the design and *modus operandi* of a nozzle that currently works in the following mode (Figure 2) when the channel walls are slightly squeezed in. The adapted nozzle should produce a microdrop of radius say 25% of the nozzle radius (and travelling at twice the speed).

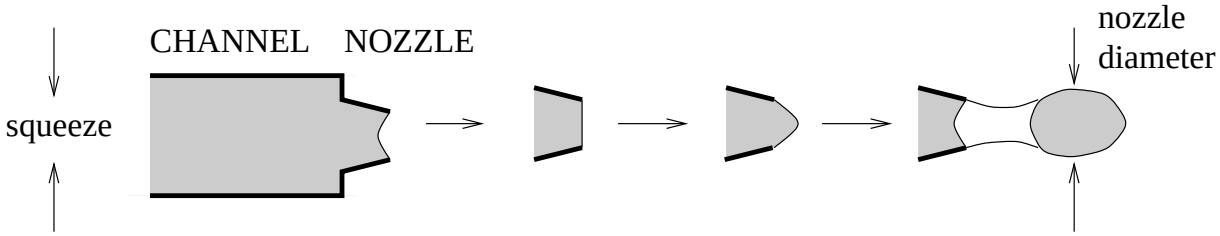

Figure 2: Schematic diagram of normal mode of operation.

The crucial physical attributes are that

(i) the ink behaves basically as an inviscid incompressible fluid during the timescale of drop ejection over the relevant nozzle length scale;

(ii) the squeeze is so small that the (small) fluid elasticity only admits linearised acoustic waves to propagate in the channel. The time of flight for these waves across the channel is very short compared to the time scale of droplet ejection;

(iii) the rise time for the application and release of the squeeze wave is very short compared to the droplet ejection time scale in the device as currently used.

There are many other phenomena that are not considered to be rate-limiting (*e.g.* channel wall elasticity, temperature-dependence of viscosity, surface tension, end wall effects *etc*).

3 First key Suggestion

Xaar's data for the droplet speed and for the ejection time scale enable the acceleration, g, of the meniscus out of the nozzle to be calculated. This acceleration points into the ink in the sucking phase of the cycle and hence destabilises the meniscus according to the Rayleigh-Taylor instability [2]. Equally, it enhances the 'effective gravity' on the pressure phase of the cycle. Thus the printer meniscus is subject to an extreme form of what is called 'Faraday Resonance', *i.e.* the resonance phenomenon that occurs in vertical oscillation of a column of liquid with a free surface.

To quantify this, consider an evolution mode of the surface meniscus $e^{i(\omega t - kx)}$ where ω is the frequency and k the wavenumber ($2\pi/k$ = wavelength), where x is distance along the meniscus. The 'dispersion relation' for such modes is

$$\omega^2 = gk + \sigma k^3/\rho \tag{1}$$

where σ is the ink surface tension, ρ is the ink density, and $g \gtrless 0$ in the pressure/suction phases respectively. Surface tension will stabilise all short wavelength (large k)

disturbances, but, when $g < 0$ and $k \sim \sqrt{-\rho g/\sigma}$, the acceleration will begin to destabilise the surface. Several calculations confirmed that this situation arises when the wavelength is comparable to the nozzle diameter.

Hence the proposed explanation for microdrop generation is via the purely 'inertia vs. surface tension' competition leading to a meniscus morphology as in Figure 3.

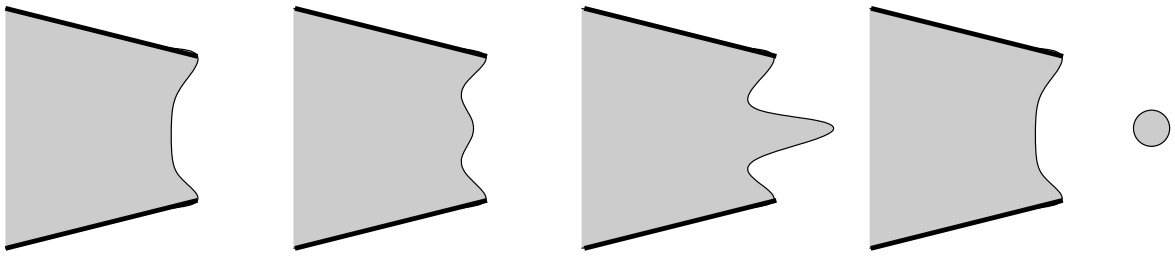

Figure 3: Desired mode of operation.

It is interesting to compare this scenario with that of the collapse of a Rayleigh bubble [3, Example XV.48]. This is also an inviscid inertial flow, described by the model illustrated in Figure 4, where ϕ is the velocity potential, $\nabla\phi$ the velocity, $\nabla^2\phi = 0$,

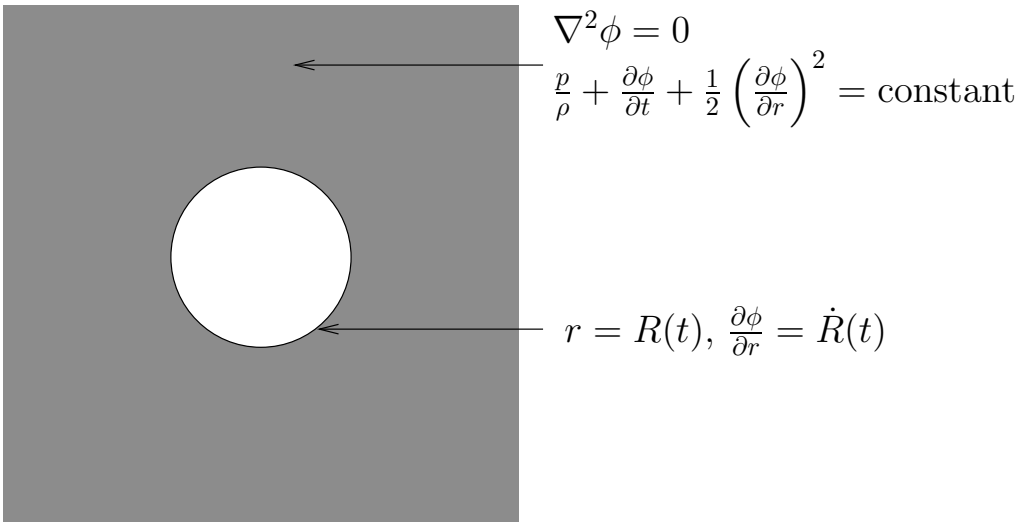

Figure 4: Model for Rayleigh bubble collapse.

$p/\rho + \partial\phi/\partial t + \frac{1}{2}(\partial\phi/\partial r)^2 = \text{constant}$ (the dynamic condition from Bernoulli's equation), with the kinematic condition $\partial\phi/\partial r = \dot{R}$ on the bubble surface $r = R(t)$, and with $|\nabla\phi| \to 0$ and $p \to p_\infty$ at infinity. (It is interesting that the ink overpressures generated in the squeeze would, were they applied to a Rayleigh bubble, cause collapse on a timescale similar to that of the drop ejection.) This gives a bubble collapse time of order $R(0)/\sqrt{p_\infty/\rho}$ when $p_\infty > 0$. However we note that whenever there is asymmetry present the bubble collapse may be far from spherical. Calculations in [4] reveal that a bubble near a wall collapses with a change of morphology as shown in Figure 5.

Alas, this mechanism does not mention the compressibility phenomena generated on the very short time scale squeezing of the channel walls! If an acoustic pulse in this ink

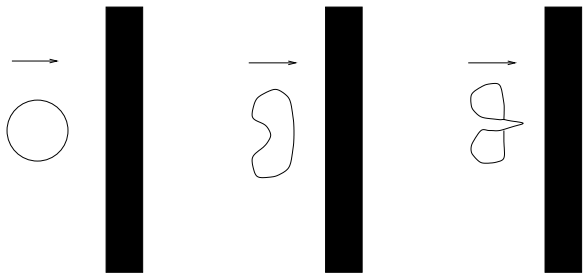

Figure 5: Schematic diagram of bubble collapse near a wall.

were to impact the meniscus in Figure 3, the wave reflection/diffraction would take place on a time-scale much too short to allow any bulk droplet motion to be generated. We will return to this in Section 6.

4 Quantifying the scenario of Figure 3

(i) A simple-minded and unrealistic approach is to consider the nozzle to be longer and more gently tapered than those used in practice and to thus assume that the meniscus is flat to lowest order. Then if $h(x)$ is the slowly-varying nozzle cross-section as in Figure 6, and the meniscus is at $x = s(t)$, the 'hydraulic model' is

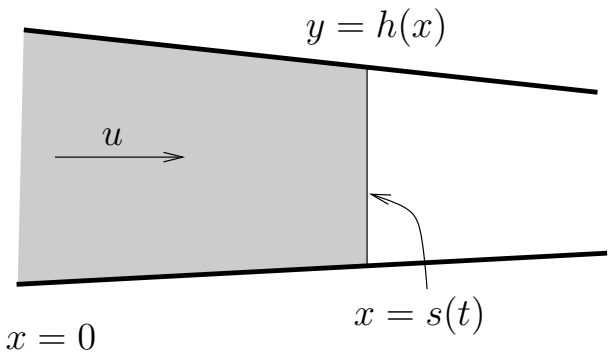

Figure 6: Hydraulic model.

$$\frac{\partial}{\partial x}(uh) = 0, \quad \rho\left(\frac{\partial u}{\partial t} + u\frac{\partial u}{\partial x}\right) = -\frac{\partial p}{\partial x} \qquad \text{with } u = \frac{ds}{dt}, \quad p = 0 \quad \text{at } x = s. \tag{2}$$

This model needs to be closed with the prescription of some driving pressure, say $P(t)$ at the nozzle entrance.

Quite apart from the difficulty of writing down $P(t)$, this model as it stands has clearly no possibility of predicting the scenario of Figure 3. However, the model does have the virtue of predicting the time-scale of drop ejection correctly (when P is the overpressure generated by Xaar) and it can be used as a starting point for the following more refined model.

(ii) The above model needs to be made fully 2-dimensional or axisymmetric and the application of the pressure drive from the channel needs to be considered more

carefully. Hence the inertial/surface tension scenario in Figure 7 is proposed (with the same notation as above). Compared to the Rayleigh bubble model, the mechanical

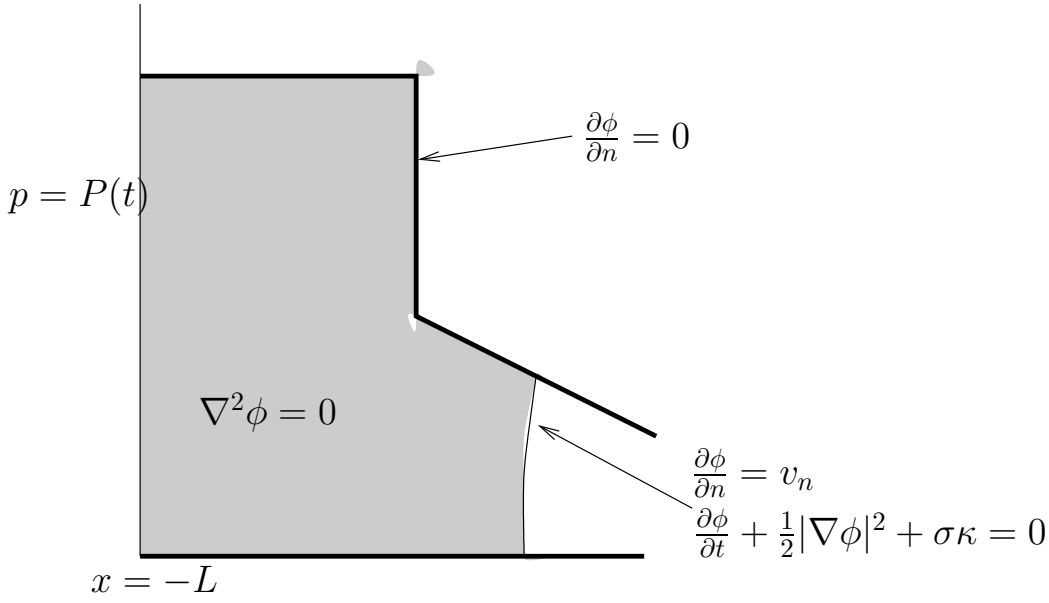

Figure 7: Two-dimensional or axisymmetric model.

boundary condition has been modified to account for surface tension and, compared to the 'hydraulic' model, the pressure is applied at a station $x = -L$. The length L is determined by the lateral extent of the incompressible 'inertia dominated' nozzle flow compared to the compressible 'acoustic' flow in the channel: we expect it to be about a channel radius but the pressure at $x = -L$ is a yet-to-be-determined function $P(t)$.

When the pressure $P(t)$ acts over a short time τ (as mentioned above, microdrops seem to be associated with short pulses), we can use a pressure impulse model to calculate the initial velocity potential. We solve $\nabla^2\phi_0 = 0$ in the fluid domain (as in Figure 7) with $\phi_0 = \int_0^\tau P(t)/\rho\, dt$ on the left-hand boundary and $\phi_0 = 0$ on the meniscus. This ignores pressures due to surface tension but if the meniscus is flat or circular this is constant anyway. The initial velocity is $\nabla\phi_0$. Figures 8 and 9 show the initial velocity for a flat and circular initial meniscus (two-dimensional calculations in MATLAB). The motion thereafter, with zero pressure at the left-hand end before the opposite pressure reversal spike, is more complex to calculate. The presence of the free surface makes it unlikely that applying the reverse impulse will reduce the fluid to rest, let alone return the system to its original configuration, but only numerical studies will reveal the evolution. It is likely that surface tension effects will be significant, and we can speculate that microdrops occur when the free surface evolves during this 'rest phase' in such a way that there is a nascent jet pointing to the right (as in the third picture of Figure 3) when the reverse spike is applied. A very rough computation of the pressure impulse in this hypothetical situation is shown in Figure 10. It indicates that the true process of jet formation may be more complicated than suggested here.

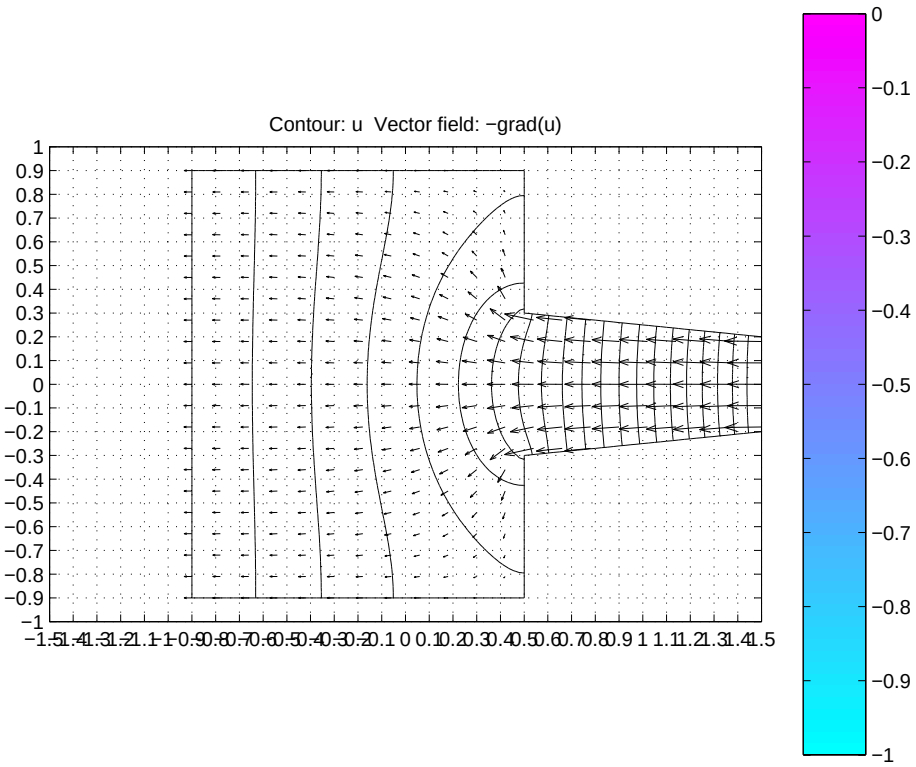

Figure 8: Initial velocity for a flat meniscus.

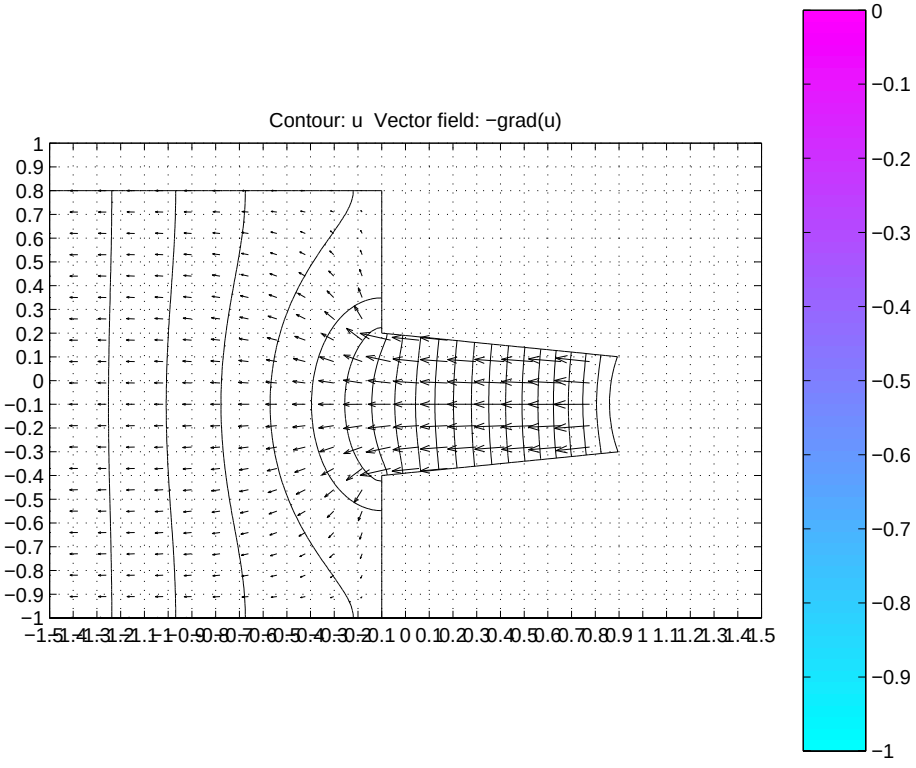

Figure 9: Initial velocity for a circular meniscus.

Remarks

- EJH says that his PhD student Richard Day has done this in his thesis. (This needs to be checked out, *e.g.* with John Lister).
- It should be possible to synthesise the above two models by using the velocity and pressure fields as calculated explicitly in (i) in the first stage of an iterative procedure in which the deviation of the meniscus from planarity is used as the small parameter. Although this will never allow us to track the evolution of any jets that may emerge, it may reveal that the most rapid evolution takes place in the middle of the meniscus as in Figure 3.
- The model (ii) still leaves open the detailed coupling between the nozzle flow and the channel flow. We recall that the time-scale for acoustic wave propagation in the channel is of order 10^{-2} compared to the nozzle flow time-scale. A possible approach to this coupling is outlined in the next section.
- The accurate numerical solution of a model such as this is going to be vital if we are to understand the consequences of the rapidly changing 'effective' gravity (in the x-direction) on the meniscus evolution. This effective gravity alternately stabilises and destabilises the meniscus and at the moment it is quite unclear at which stage of the cycle jet formation leading to microdrops is most likely.

5 Scaling analysis for the matching problem

Despite the fact that timescales are exceedingly short and that the actuator is understood in terms of acoustic waves, the proposed nozzle analysis uses quasi-static, incompressible fluid dynamics. To reconcile this with acoustic behaviour within the channel, a matched asymptotic procedure appears to be called for (so resolving the ambiguity about choosing $P(t)$ in Section 3). The following (somewhat idealized) scaling analysis indicates this procedure, focusing particularly upon the nozzle and its vicinity.

To replace physical variables (denoted by tildes) in the (compressible) Navier-Stokes equations, dimensionless variables are based upon the round-trip time $2t_0$ for acoustic waves travelling along the actuator channel, the nozzle exit radius a and the bulk modulus $B\rho_0$ of the ink. At operating pressures, the fractional change in ink density $\approx 10^{-4}$, so that using

$$\tilde{\mathbf{x}} = a\mathbf{x}\,, \quad \tilde{t} = t_0 t\,, \quad \tilde{\mathbf{u}} = a t_0^{-1}\mathbf{u}\,, \quad \tilde{\rho} = \rho_0(1+\varepsilon p)\,, \quad \tilde{p} = p_0 + \rho_0 B\varepsilon p$$

yields

$$\nabla\cdot\mathbf{u} + \varepsilon\left(\frac{\partial p}{\partial t} + (\mathbf{u}\cdot\nabla)p + p\nabla\cdot\mathbf{u}\right) = 0\,, \tag{3}$$

$$(1+\varepsilon p)\left(\frac{\partial \mathbf{u}}{\partial t} + (\mathbf{u}\cdot\nabla)\mathbf{u}\right) + \nabla p = \frac{\mu t_0}{\rho_0 a^2}\left(\nabla^2\mathbf{u} + \mu'\nabla(\nabla\cdot\mathbf{u})\right)\,, \tag{4}$$

when the small parameter ε is chosen as $\varepsilon = a^2/(Bt_0^2)$. Since $B = (d\tilde{p}/d\tilde{\rho})_0 = c_0^2$, where the acoustic speed is $c_0 \simeq 1200$ m/sec but $c_0 t_0 \simeq 1.5b$ (b = channel length) due

to wall elasticity, then $\varepsilon = a^2/(c_0 t_0)^2 \sim 0.5 \times 10^{-4}$ as required. The Reynolds number $\mathrm{Re} = \rho_0 a^2/\mu t_0$ is around 120, so that $\mu t_0/(\rho_0 a^2) \equiv \delta$ is small ($\approx \varepsilon^{1/2}$), while the viscosity ratio μ' is O(1).

To leading order, flow is irrotational so allowing $\mathbf{u} = \nabla\phi + \mathrm{O}(\delta)$. Then, as in Section 3, the flow within the nozzle is approximated by quasi-static flows governed by Laplace's equation $\nabla^2\phi = 0$ with an appropriate capillary boundary condition at the free surface and with $\nabla\phi \to U_0(t)\mathbf{i}$ as $x \to -\infty$ within the channel (as in Figs. 8-10). Within this nozzle region, the pressure is given by the unsteady version of Bernoulli's Law

$$p + \frac{\partial\phi}{\partial t} + \frac{1}{2}\left|\nabla\phi\right|^2 = 0.$$

At each instant t, the potential $\phi(\mathbf{x}, t)$, velocity field $\mathbf{u} = \nabla\phi$ and pressure field $p(\mathbf{x}, t)$ are determined instantaneously, so yielding $p \sim -x\dot{U}_0(t) + p_1(t)$ as $x \to -\infty$, with $p_1(t)$ being determined at each instant from the flow field and free-surface geometry. This one-dimensional behaviour should provide the (nonlinear) impedance end-condition for acoustic waves in the channel. Fluid momentum within the nozzle will be involved in the calculation of $p_1(t)$.

An important modification arises during the short intervals in which acoustic pressure varies rapidly. This is demonstrated by writing $t = t_c + \varepsilon^{1/2}\tau$, $\mathbf{u} = \nabla\phi + \varepsilon^{1/2}\nabla\hat{\phi}$ with $\hat{\phi} = \hat{\phi}(\mathbf{x}, \tau)$ so yielding, to leading order,

$$\nabla^2\hat{\phi} = -\partial p/\partial\tau \ , \qquad p = -\partial\phi/\partial t - \partial\hat{\phi}/\partial\tau \ .$$

Consequently, the rapid variations, even within the nozzle, are acoustic, being governed by $\nabla^2\hat{\phi} = \hat{\phi}_{tt}$. However, this regime is of short duration and is associated with small perturbations to the velocity field. It is unlikely to significantly affect calculations of nozzle and droplet momentum (but could, if critically timed, be important in determining evolution of the free surface).

Slender nozzle analysis. Some features of the foregoing analysis are simply demonstrated by a further approximation based on the small inclination α (~ 0.2) of the nozzle wall. This hydraulic model (cf. Section 3) is of dubious numerical validity since the channel length hardly exceeds the outlet diameter. Nevertheless, an axisymmetric analysis readily demonstrates how the expected crucial physical features predominate.

For a slender nozzle, it would be appropriate to introduce a stretched axial coordinate $z \equiv \alpha x$ and, using cylindrical polars, to write the nozzle wall as $r = R(z)$, with $R'(z) = \mathrm{O}(1)$. Using axial and radial velocity components $u(r, z, t)$ and $\alpha v(r, z, t)$ with pressure $p = \alpha^{-1}\bar{p}(r, z, t)$ then gives, from (3) and (4),

$$\frac{\partial u}{\partial z} + \frac{1}{r}\frac{\partial(rv)}{\partial r} + \varepsilon\alpha^{-2}\frac{\partial\bar{p}}{\partial t} + \varepsilon\alpha^{-1}\left(\frac{\partial(\bar{p}u)}{\partial z} + \frac{1}{r}\frac{\partial(r\bar{p}v)}{\partial r}\right) = 0\,, \tag{5}$$

$$\frac{\partial u}{\partial t} + \frac{\partial\bar{p}}{\partial z} + \alpha\left(u\frac{\partial u}{\partial z} + v\frac{\partial u}{\partial r}\right) = \delta\left(\frac{1}{r}\frac{\partial(ru_r)}{\partial r} + \alpha^2\frac{\partial^2 u}{\partial z^2}\right) + \mathrm{O}(\varepsilon\alpha^{-1})\,, \tag{6}$$

$$\frac{\partial\bar{p}}{\partial r} + \alpha^2\left(\frac{\partial v}{\partial t} + \alpha u\frac{\partial v}{\partial z} + \alpha v\frac{\partial v}{\partial r}\right) = \alpha^2\delta\left(\frac{1}{r}\frac{\partial(rv_r)}{\partial r} + \alpha^2\frac{\partial^2 v}{\partial z^2}\right) + \mathrm{O}(\varepsilon\alpha)\,. \tag{7}$$

As usual, the leading order solution has $\bar{p} \sim p_0(z,t)$, $u \sim u_0(z,t)$, with $v \sim v_0 = -\frac{1}{2} r u_{0,z}$. Since the cross-sectional area is $A = A(z) = \pi R^2(z)$, the boundary conditions at $r = R(z)$ give

$$u_0(z,t) = \frac{Q(t)}{R^2(z)}\,, \quad v_0(r,z,t) = r\frac{R'(z)}{R^3(z)}Q(t) \quad \text{and} \quad p_0(z,t) = -Q'(t)\int \frac{dz}{R^2(z)} + P_0(t)\,.$$

This shows how the pressure difference across the nozzle is balanced by the rate of change of fluid momentum within the nozzle. The $\mathrm{O}(\alpha)$ advected term from (6) gives a correction $\alpha Q^2(t) R^{-5} R'(z)$ to $-\partial\bar{p}/\partial z$, but does not alter the one-dimensionality of the solution. Curvature of the meniscus, introducing dependence of $\bar{p}$ on r, is not adequately treated by this scaling.

However, to accommodate rapid pressure fluctuations, rescaling time by $t = t_c + \varepsilon^{1/2}\alpha^{-1}\tau$ with $u = u_0(z,t) + \varepsilon^{1/2}\alpha^{-1}\hat{u}(r,z,t)$, $v = \alpha v_0(r,z,t) + \varepsilon^{1/2}\hat{v}(r,z,\tau)$ and $\bar{p} = p_0(z,t) + \hat{p}(r,z,\tau)$ gives the leading order equations

$$\frac{\partial\hat{u}_0}{\partial z} + \frac{1}{r}\frac{\partial(r\hat{v}_0)}{\partial r} + \frac{\partial\hat{p}_0}{\partial\tau} = 0\,, \quad \frac{\partial\hat{u}_0}{\partial\tau} + \frac{\partial\hat{p}_0}{\partial z} = 0\,, \quad \frac{\partial\hat{p}_0}{\partial r} = 0$$

for which appropriate solutions have the form

$$\hat{p}_0 = \hat{p}_0(z,\tau)\,, \quad \hat{u}_0 = \hat{u}_0(z,\tau)\,, \quad \hat{v}_0 = r\hat{u}_0(z,t)R'(z)/R(z)$$

(describing flow with self-similar streamlines). Writing $\hat{u}_0 = \hat{\phi}_z$ and $\hat{p}_0 = -\hat{\phi}_\tau$, it is found that the acoustic potential $\hat{\phi}(z,\tau)$ must satisfy

$$R(z)\hat{\phi}_{zz} + 2R'(z)\hat{\phi}_z = R(z)\hat{\phi}_{\tau\tau}\,.$$

For the special case of conical nozzles ($R''(z) = 0$), this becomes the usual wave equation for $R(z)\hat{\phi}(z,\tau)$ with *general solution*

$$\hat{\phi} = \{f(\tau - z) + g(\tau + z)\}/R(z)\,, \tag{8}$$

which should be useful in describing how a rapid ramp increase in pressure traverses the nozzle to impact upon the meniscus (even though the meniscus curvature will make the reflected wave have more complicated geometry).

6 Acoustic model

As the squeeze wave is initiated, planar compressional waves will be repeatedly reflected back and forth across the channel over most of its length. These waves will be diffracted in a more complicated process near the nozzle which, for the purposes of the analysis in the main part of the channel, may be modelled as a time-varying impedance boundary condition.

The hope is that, whereas the effect of a single pressure pulse moving rapidly towards the nozzle could never generate bulk motion (Section 3), the *cumulative* effect of the interacting pressure pulses in the channel together with any damping mechanism that

may be present will be enough to rectify the pressure profile as seen by the nozzle from the first sketch of Figure 11 to the second.

Depending on whether or not this acoustic modelling reveals any 'impedance behaviour' near the nozzle, the boundary condition at $x = -L$ in (ii) above may need modification.

In any event the key mechanism for the transfer of energy and momentum from the acoustic field to the droplet seems to be the emergence of a pressure rise near the nozzle that is gradual enough to be appropriate to the inertial flow model.

7 Further comments

We close with two further remarks:

(i) Xaar have observed that when the squeeze voltage is large enough for droplets to be ejected, their velocity depends linearly on voltage (assuming the voltage is high enough for the ligature connecting the droplet to the nozzle to be broken). Moreover, for smaller voltages in which no drop is ejected, but rather an outwardly bulged meniscus, the meniscus size is also linearly dependent on voltage.

Note that all the nozzle flow models proposed here are nonlinear.

(ii) Many other flow regimes await attention. To take just two examples, the ligature dynamics requires consideration of Rayleigh neck off and extensional (Trouton) viscosity, while the possibility of differential temperatures around the nozzle orifice may allow control over droplet trajectories that may not be normal to the nozzle.

References

[1] Dai Huang and Eun Sok Kim, *Micromachined acoustic-wave liquid ejector*, Journal of Microelectromechanical Systems, **10**(3) 442–449 (2001).

[2] P. G. Drazin and W. H. Reid, *Hydrodynamic Stability*, Cambridge University Press, 1981.

[3] L. M. Milne-Thomson, *Theoretical Hydrodynamics* (Second edition), MacMillan, London, 1949.

[4] J. P. Best and J. R. Blake, *An estimate of the Kelvin impulse of a transient cavity*, Journal of Fluid Mechanics, **261** 75–93 (1994).

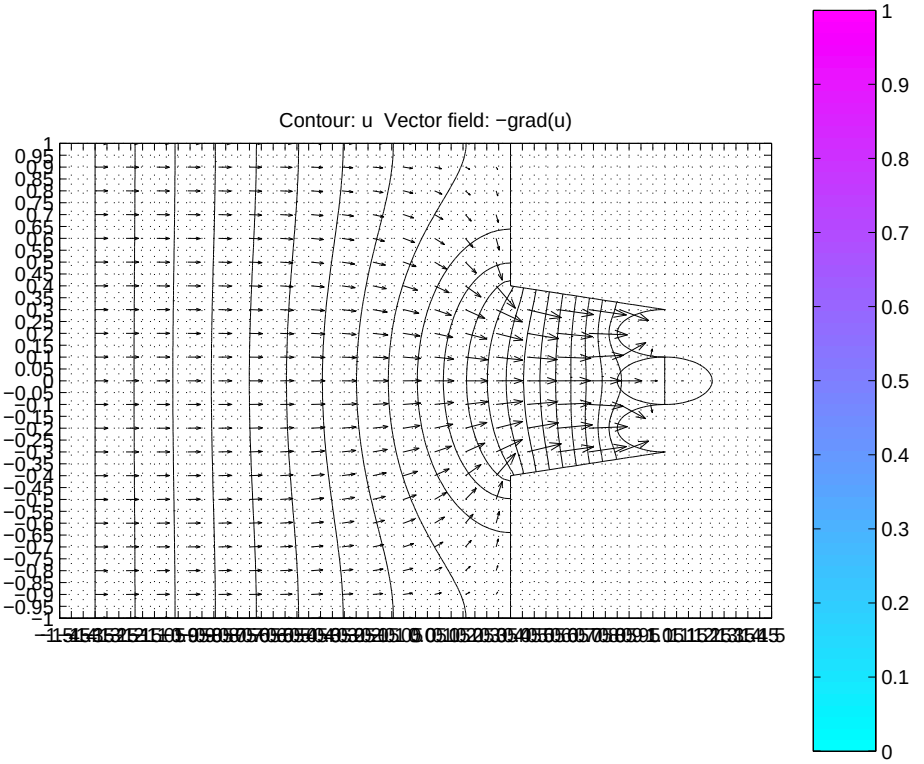

Figure 10: Rough computation of pressure impulse.

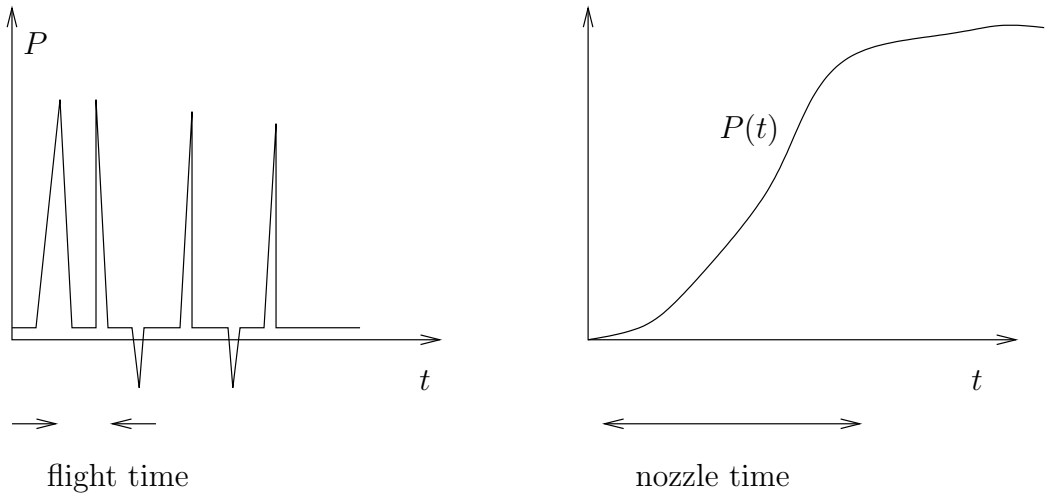

Figure 11: Pressure profiles.